# Early warning signals of desertification transitions in semiarid ecosystems

Raffaele Corrado,[1,*] Anna Maria Cherubini,[2,†] and Cecilia Pennetta[2,3,‡]
[1]*PhD School on Climate Change Sciences, University of Salento, I-73100 Lecce, Italy*
[2]*Dipartimento di Matematica e Fisica "Ennio De Giorgi," University of Salento, I-73100 Lecce, Italy*
[3]*Istituto Nazionale di Fisica Nucleare (INFN), Italy*
(Received 7 February 2014; revised manuscript received 6 August 2014; published 4 December 2014)

The identification of early warning signals for regime shifts in ecosystems is of crucial importance given their impact in terms of economic and social effects. We present here the results of a theoretical study on the desertification transition in semiarid ecosystems under external stress. We performed numerical simulations based on a stochastic cellular automaton model, and we studied the dynamics of the vegetation clusters in terms of percolation theory, assumed as an effective tool for analyzing the geometrical properties of the clusters. Focusing on the role played by the strength of external stresses, measured by the mortality rate $m$, we followed the progressive degradation of the ecosystem for increasing $m$, identifying different stages: first, the fragmentation transition occurring at relatively low values of $m$, then the desertification transition at higher mortality rates, and finally the full desertification transition corresponding to the extinction of the vegetation and the almost complete degradation of the soil, attained at the maximum value of $m$. For each transition we calculated the spanning probabilities as functions of $m$ and the percolation thresholds according to different spanning criteria. The identification of the different thresholds is proposed as an useful tool for monitoring the increasing degradation of real-world finite-size systems. Moreover, we studied the time fluctuations of the sizes of the biggest clusters of vegetated and nonvegetated cells over the entire range of mortality values. The change of sign in the skewness of the size distributions, occurring at the fragmentation threshold for the biggest vegetation cluster and at the desertification threshold for the nonvegetated cluster, offers new early warning signals for desertification. Other new and robust indicators are given by the maxima of the root-mean-square deviation of the distributions, which are attained respectively inside the fragmentation interval, for the vegetated biggest cluster, and inside the desertification interval, for the nonvegetated cluster.

DOI: 10.1103/PhysRevE.90.062705 PACS number(s): 87.23.Cc, 87.10.Mn, 92.40.Iv, 64.60.ah

## I. INTRODUCTION

Drylands, i.e., regions where water shortage limits the vegetation growth, cover a significant portion of earth land area (about 41%) [1,2]. They are defined in terms of the so-called aridity index (AI) [1,2] and can be classified as dry subumid, semiarid, arid, or hyperarid lands [1,2]. Moreover, they include several biomes such as deserts, grasslands, Mediterranean shrublands, and forests, with different destination (rangelands, croplands, urban, etc.) [1,2]. They are frequently characterized by a vegetation pattern that consists of a mosaic of bare soil and vegetation patches [1–5]. Dryland habitats are fragile and can undergo regime shifts when exposed to strong external stresses, such as an exceeding anthropogenic load or an increased frequency of extreme climatic events [1–8].

An important case of regime shift is the desertification transition [1–4,9–12], which implies a huge and often irreversible loss of ecological and economic resources [1,2]. Many studies in the literature pointed out the role of vegetation patchiness as an essential tool to assess the desertification risk and identify early warning signals of desertification [3,4,9–33]. This is particularly relevant for applications, because spatial indicators directly related to vegetation patterns can be accurately measured through collected data and analyzed by several efficient systems now available [19–25].

Examples of systems suitable for monitoring changes in vegetation in ecosystems at risk are the CLASlite system, introduced for processing output from satellite sensors and specifically designed to provide mapping of vegetation (see Ref. [20] for its use in monitoring tropical forests degradation) or the LiDAR (light detection and ranging) technique, which provides three-dimensional data for vegetation structure and spatial patterns (see in particular Refs. [21] and [24] for spatial analysis of Peruvian Amazon and Ref. [22] for the study of rate and spatial patterns of treefall in a savanna-type landscape). Other systems, such as the VSWIR (visible-to-shortwave infrared spectrometry) can provide data on chemical compositions and water content (for example, see Ref. [23] for an application to a Mediterranean-type ecosystem).

Concerning desertification models, for the purpose of this paper we mention in particular the stochastic cellular automatom (SCA) model introduced in Ref. [10]. This model takes into account different ecological mechanisms, and it can be used to describe several ecological landscapes. Its predictions concerning the change in the vegetation patch-size distribution near the desertification transition were validated by field data collected in three Mediterranean arid ecosystems subject to grazing [9]. In particular, both simulated and observed vegetation patterns exhibit a patch-size distribution $\Pi(s)$ which deviates from a power law and shows an exponential cutoff at increasing values of the mortality rate $m$, a parameter measuring the strength of the external stress. The emergence of the cutoff was proposed by the authors as an early

*Present address: Istituto di Scienze dell'Atmosfera e del Clima, CNR, I-73100 Lecce, Italy; r.corrado@le.isac.cnr.it
†Currently on leave at Department of Mathematics, Imperial College London, SW7 2AZ London, UK; anna.cherubini@unisalento.it
‡Corresponding author: cecilia.pennetta@unisalento.it

 

indicator of desertification [9]. This behavior of the spatial distribution was successively explained by Manor and Shnerb in terms of a two-states birth-death model [34,35].

We used the SCA model in Ref. [10] to simulate a semiarid ecosystem with sufficiently realistic patchiness dynamics, and we analyzed the geometrical properties of the vegetation clusters in terms of percolation theory. Moreover we associated the desertification process with the percolation of a phase made of empty and degraded regions opposed to the "green" phase, corresponding to regions covered by vegetation. In the following we show that a percolative analysis of the geometry of the clusters [37–42] is a powerful tool for the study of desertification and allows the definition of several new early warning signals. In other terms we show that a geometric characterization of the patchiness generated by the "true" system's dynamics can be very effective for understanding some basic features of the desertification process, leading to the identification of new transition indicators, including very early ones.

The organization of the paper is the following: Sec. II describes the theoretical and numerical methods adopted, including a short discussion of the model [10] used for the numerical simulations. Section III presents and discusses in detail our results, and Sec. IV recaps the conclusions.

## II. METHOD

We described a semiarid ecosystem by numerical simulations based on the SCA model introduced in Ref. [10]. This choice was motivated by the ability of this model to provide sufficiently realistic patchiness dynamics, accounting for several biological and geophysical mechanisms acting on drylands and by its rich phenomenology, covering several ecological scenarios [9,10,19,43]. Here we only outline some basic features of the model, while we refer to the original papers for a full description [9,10].

A given ecosystem was modeled as a three states SCA [36]. Each cell of the $N \times N$ square lattice can be found probabilistically in one of the following three states: a vegetation covered state denoted by $\{+\}$ (living cell), a state in which the cell is empty but colonizable by vegetation denoted by $\{0\}$ (dead cell), and an empty and degraded state denoted by $\{-\}$ (degraded cell). A degraded cell cannot be colonized before being recovered, thus the transition $\{-\} \to \{+\}$ is forbidden, similarly for the reverse transition. The allowed transitions occur stochastically with rates

$$W_{+0} = m, \tag{1}$$

$$W_{0+} = [\delta\rho_+ + (1-\delta)q_{+|0}](b - c\rho_+), \tag{2}$$

$$W_{0-} = d, \tag{3}$$

$$W_{-0} = r + f q_{+|-}. \tag{4}$$

Equations (1), (2), (3), and (4) define, respectively, the mortality, colonization, degradation, and recovery processes.

The mortality rate $m$ measures the strength of the external stress, and it has been taken here as the control (driving) parameter of the transition. The global vegetation mass fraction or living cells density $\rho_+$ (i.e., total number of living cells normalized to the total number of lattice cells) plays the role of order parameter of the transition. The other quantities appearing in Eqs. (1)–(4) have the following meaning: $q_{i|j}$ is the fraction of first neighbors in the state $\{i\}$ around a cell in the state $\{j\}$; $\delta$ represents the fraction of seeds globally dispersed by wind, animals, etc.; $b$ is the colonization parameter, associated with several intrinsic properties of a vegetated cell, such as seed production rate, seed survival, germination, and survival probabilities (intrinsic properties because $b$ does not include global competition effects among plants). The strength of the last effects is instead determined by $c$. The parameter $d$ gives the rate of soil degradation and it accounts for the intrinsic soil characteristics, climatics and/or anthropogenic factors. $f$ is the local facilitation parameter which describes local cooperative interactions among plants and positive feedback between soil and plants. Finally, $r$ is the spontaneous regenerative rate of a degraded cell in absence of vegetation covering the first neighbor cells. The results presented in this paper were obtained by taking $b = 0.6$, $c = 0.3$, $d = 0.2$, $\delta = 0.1$, $f = 0.9$, and $r = 0.0004$. These values of the parameters were chosen as reasonable values to simulate "real-world" field data [9,19]. Except when differently stated, we considered lattices of linear size $N = 100$.

In the numerical simulations each iteration step (a synchronous update of the states of all the lattice cells) was associated with an elementary time step in an appropriate time scale. Therefore the transition rates, which are transition probabilities in the unit of time, are expressed in arbitrary units. In practical applications, the choice of the time unit depends on which plants live in the given ecosystem and on the time scales characterizing their living cycles; thus the time unit can vary from a week to some months. In this way, we simulated the time evolution of an ecosystem, and we generated time series for several quantities, such as the densities of cells in each of the three states, $\rho_+(t)$, $\rho_0(t)$, $\rho_-(t) = 1 - \rho_+(t) - \rho_0(t)$, or the size of the biggest cluster of living (dead, degraded) cells, $S_{\mathrm{MAX}}(t)$.

The recognition and counting of the clusters were based on the Hoshen-Kopelman algorithm [44]. We used periodic boundary conditions only for the calculation of the transition rates, while the cluster connectivity was evaluated on the finite $N \times N$ lattice. The simulations were performed starting with an initial state corresponding to given concentrations, $\rho_+(t_0)$, $\rho_0(t_0)$ of randomly distributed cells. The initial values for the densities were $\rho_+(t_0) = 0.5$, $\rho_0(t_0) = 0.2$, but we checked that these values do not affect the statistical properties of the stationary regime reached at the relaxation of the initial transient. The time series statistical analysis concerned only the stationary portion of the signal, after the relaxation of the initial transient [43]. The typical length of the time series was $1\text{–}5 \times 10^4$ records.

We stress the fact that the state of the whole system at a given time step is determined (probabilistically) by Eqs. (1)–(4), which control its dynamics evolution, according to a Markovian chain. Thus, the structure of the vegetation clusters (size, number, and position) reflects only the system's dynamics. Nevertheless in order to extract fruitful information from such a complex system, identifying new early desertification indicators, we introduced a percolation framework which allows a more effective analysis of the geometrical properties

of the different patches [37–42]. The percolation process described here is different from the standard uncorrelated one [37,38], occurring with uniform probability, being a correlated percolation, consistently with Eqs. (1)–(4).

It must be also noted that the difference between dead and degraded cells is a key feature of the model, necessary for a suitable modeling of the ecological dynamics, given the different biological and geophysical role of simply unoccupied or degraded soil areas. However, new and interesting insights into the desertification transition can be obtained by applying a percolation analysis to a two-phase system, made of living and nonliving cells. In any case, in doing so, we are not changing the three-states dynamical system but we are only applying a simplified but useful interpretation scheme of its behavior. Therefore we denote the density of nonliving cells by $\rho_{0,-} \equiv \rho_0 + \rho_-$.

Moreover, since the cluster connectivity criterium is based on first neighbors (two cells belong to the same cluster either if they share at least a side, first neighbor cells, or if they are connected by a continuous path of such cells) there can be instances, for some conditions and particular lattice configurations, where no phase percolates. When this happens neither living nor nonliving cells give rise to an incipient percolating cluster spanning through the lattice: these configurations can be seen as the point of maximum instability for the system, corresponding to the maximum mixing between the two phases.

On the other hand there are several spanning criteria [39,40]. Therefore we calculated the different probabilities $R_N(\rho_+)$ for a cluster of living cells to span a $N \times N$ lattice according to each of them. Similarly, we also considered the different spanning probabilities $R_N(\rho_{0,-})$ for a cluster of nonliving cells. In the following we drop the subindex $N$ because all the probabilities $R$ reported in this paper were obtained for $N = 100$. In particular, we calculated the probabilities $R_b$, $R_h$, $R_e$, $R_1$, hereafter defined: $R_b$ is the probability of existence of a cluster spanning the lattice along both directions (horizontal $h$ and vertical $v$) simultaneously; $R_h$ is the probability of spanning along a given direction (horizontal), where $R_h = R_v$ (probability of spanning along a vertical direction) being the model isotropic, at least for initial conditions corresponding to a random pattern, which is the case studied here. $R_e$ is the probability of spanning along either direction, while $R_1$ is the probability of spanning along one direction but not the other, where $R_e = 2R_h - R_b$ and $R_1 = R_h - R_b$ [39,40]. The calculation of the two independent probabilities $R_b$ and $R_h$ was performed by counting the frequency of existence of a spanning cluster over $N_c = 8 \times 10^4$ lattice configurations in the same conditions [the same parameter values and same initial concentrations $\rho_+(t_0)$, $\rho_0(t_0)$]. Given the spanning probabilities as functions of the densities $\rho_+$ and $\rho_{0,-}$, the finite-size percolation thresholds for living and nonliving cells, respectively, for any percolation criterium can be computed by [37,41]

$$p_{av(N)} = \langle \rho \rangle = 1 - \int_0^1 R_N(\rho)\, d\rho. \tag{5}$$

Equation (5) provides the average value of the threshold for a finite system of linear size $N$. All these thresholds converge for $N \to \infty$ to a unique percolation threshold $p_c \equiv \lim_{N\to\infty} p_{av(N)}$ [37,39,40]. Nevertheless, for finite-size real-world systems the existence and the identification of the different thresholds provide a way to follow closely the degradation process of the ecosystem. Further details concerning the calculation of specific quantities will be given in Sec. III.

## III. RESULTS

We present here the results of numerical simulations of an ecosystem under external pressure due to anthropogenic factors or climate shifts or any other environmental stress acting on the vegetation mortality rate. In particular, we report the results of a set of simulations performed by varying the mortality rate and taking the values specified in Sec. II for the other model parameters. These values were chosen as reasonable values to simulate "real-world" field data [9,19].

Figure 1 displays typical time evolutions of the order parameter, the living cell density $\rho_+(t)$, for increasing values of the mortality rate $m$. The plot shows qualitatively some general features characterizing the role of $m$. Namely, increasing strength of the external stress implies (1) a steady state with progressively smaller average density of vegetated cells $\langle \rho_+ \rangle$; (2) a strong raise of the amplitude of the fluctuations, $\Delta\rho_+(t) = \rho_+(t) - \langle \rho_+ \rangle$; (3) a fast growth of the relaxation time associated with the decay of the initial transient and the achievement of the steady state (which can be seen more explicitly looking at the autocorrelation times for increasing $m$) [45].

### A. Full desertification transition

At increasing mortality rate, there exists a value $m_c$ above which the steady state of the system corresponds to $\langle \rho_+ \rangle = 0$, i.e., at $m_c$ the system undergoes a transition associated with

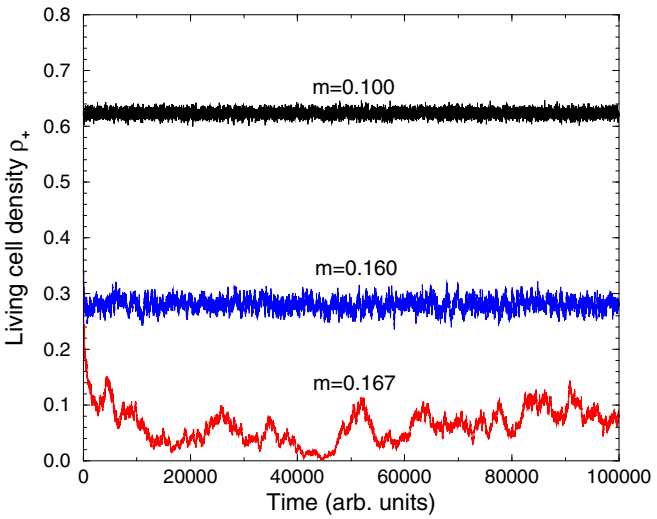


FIG. 1. (Color online) Typical time evolution of the living cell density $\rho_+(t)$ for increasing mortality rate $m$. From top to bottom: $m = 0.1000$ (black), $m = 0.1600$ (blue), $m = 0.1670$ (red). The linear lattice size is $N = 100$; the other parameters are fixed (see text). The time unit is one iteration step.

TABLE I. Critical mortality rate $m_c$ associated with the full desertification transition for increasing lattice size $N$.

| $m_c$ | $N$ |
|---|---|
| $0.1672 \pm 0.0001$ | 50 |
| $0.1683 \pm 0.0001$ | 100 |
| $0.1685 \pm 0.0001$ | 150 |
| $0.1686 \pm 0.0001$ | $\lim_{N\to\infty}$ |

a full extinction of the vegetation [10] and a nearly complete degradation of the soil (the extent of the final soil degradation is determined by the parameters $d$ and $r$). We call this transition at $m_c$ *full desertification transition*. The value of $m_c$ depends on the system size and on the values of the other parameters [46]: for the set of parameters adopted here the $m_c$ values are reported in Table I as a function of $N$.

A visualization of the clustering properties in this system is given in Fig. 2 which shows a typical vegetation pattern for an arid ecosystem close to desertification. For a value of the mortality rate $m = 0.1680$, close to $m_c$, a big spanning cluster of degraded cells (dark gray or red online) covers a very large surface of the system, while vegetated cells (light gray or green online) aggregate in small clusters and dead cells (black) are mainly confined at the interface between vegetated and degraded regions.

We notice that the SCA model can describe several ecological scenarios: depending on the regions of the parameter space it can provide abrupt (first order) transitions, continuous or nearly continuous (second order) transitions, and bistable behaviors [9,10,19,43]. To identify the character of the full desertification transition at $m_c$ corresponding to our set of parameters, we analyzed the behaviors of $\langle\rho_+\rangle$ and $\sigma_{\rho_+}$, root-mean-square deviation of the $\rho_+$ fluctuations, as functions of the mortality rate. The insets of Figs. 3 and 4, respectively, plot $\langle\rho_+\rangle$ and $\sigma_{\rho_+}$ versus $m$ on linear scales. We can see

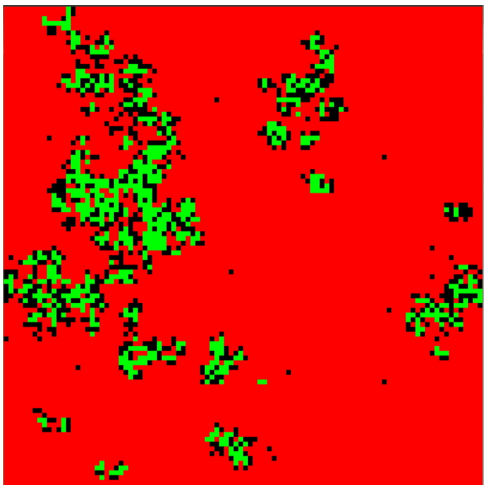

FIG. 2. (Color online) Typical vegetation pattern for a lattice of linear size $N = 100$ at $m = 0.1680$ (see the text for the values of the other parameters). The light gray (green) cells correspond to areas with vegetation, the black cells to unoccupied areas, and the dark gray (red) ones to degraded areas.

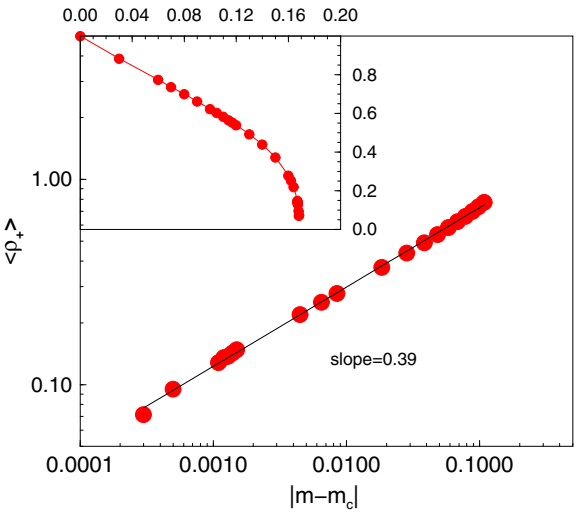


FIG. 3. (Color online) Log-log plot of the average density of living cells $\langle\rho_+\rangle$ as a function of $|m - m_c|$. Red circles correspond to numerical data, the black solid line to the the best fit, namely, a power law with slope $\beta = 0.39 \pm 0.01$. The inset displays $\langle\rho_+\rangle$ vs $m$ in a linear scale ($m$ is in arbitrary units).

that for increasing $m$ the average density approaches zero, pointing out a continuous or nearly continuous transition (it is rather difficult to establish by numerical simulations whether a transition is really continuous or discontinuous). On the contrary $\sigma_{\rho_+}$ sharply increases approaching $m_c$. This behavior is expected in any case; indeed, the increase of the variance $\sigma^2_{\rho_+}$ is a well-recognized indicator of transition [19,31]. However, the drawback is that this increase occurs at a rather advanced stage of degradation of the ecosystem.

Figure 3 also reports $\langle\rho_+\rangle$ on a log-log plot versus $|m - m_c|$: an excellent best-fit of the numerical data (red circles) is obtained with a power law of slope $0.39 \pm 0.01$. The log-log plot of $\sigma_{\rho_+}$ as a function of $|1 - \frac{m_c}{m}|$ is instead shown in Fig. 4.

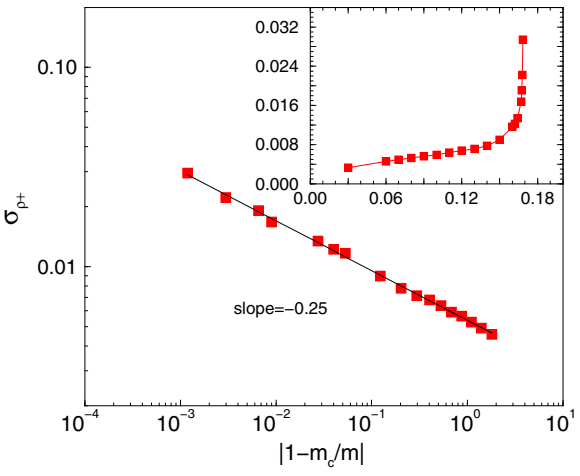


FIG. 4. (Color online) Log-log plot of the root-mean-square deviation of the living cells density, $\sigma_{\rho_+}$ vs $|1 - m_c/m|$. Red squares correspond to numerical data, the black solid line to the the best fit, i.e., to a power law with slope $-\gamma'_\sigma = -0.25 \pm 0.01$. The inset displays $\sigma_{\rho_+}$ vs $m$ in a linear scale ($m$ is in arbitrary units).

Now the numerical data (red squares) are well fitted by a power law of slope $-0.25 \pm 0.01$. Thus,

$$\langle \rho_+ \rangle = C_\rho |m - m_c|^\beta, \tag{6}$$

$$\sigma_{\rho_+} = C_\sigma \left| 1 - \frac{m_c}{m} \right|^{-\gamma'_\sigma}, \tag{7}$$

where $\beta = 0.39 \pm 0.01$ and $\gamma'_\sigma = 0.25 \pm 0.01$. The power-law behavior of $\langle \rho_+ \rangle$ and $\sigma_{\rho_+}$, associated with the critical transition at $m_c$, is controlled by the two critical exponents $\beta$ and $\gamma'_\sigma$, which determine the universality properties of the model [38,47]. It must be noted that a desertification process can be seen in general as a sort of damage spreading (DS) process [47–49]. It is well known that many DS transitions belong to the directed percolation (DP) universality class under certain rather general conditions [47–49]. In the present case, the values of $\beta$ and $\gamma'_\sigma$ significantly differ from the values reported in the literature for the corresponding exponents of the DP class in two-dimensional systems: $\beta = 0.583 \div 0.584$ and $\gamma'_\sigma = 0.15$–$0.18$ [47–51]. Moreover the critical exponents are found dependent on the model parameters [46]. As a general conclusion concerning this point, we can say that the SCA model provides nonuniversal exponents. The reasons of this nonuniversality and the connection with DP will be investigated elsewhere [46].

The critical character of the full desertification transition is also confirmed by considering the fluctuation distribution of the size of the biggest cluster of vegetated cells. We calculated the probability density function (PDF) of the distribution of the fluctuations $\Delta S_{\mathrm{MAX}}(t) \equiv S_{\mathrm{MAX}}(t) - \langle S_{\mathrm{MAX}} \rangle$, for different sizes of the system and several values of the mortality rate. This PDF is here denoted as $\phi_{S\mathrm{MAX}}$. In Fig. 5 the product $\sigma_{S\mathrm{MAX}}\ \phi_{S\mathrm{MAX}}$ is plotted as a function of the normalized fluctuation $\Delta S_{\mathrm{MAX}}(t)/\sigma_{S\mathrm{MAX}}$, where $\sigma_{S\mathrm{MAX}}$ is the root-mean-square deviation of $\Delta S_{\mathrm{MAX}}$ (this normalized representation is particularly convenient for comparing PDFs; see Refs. [52–55]). In particular, the probability densities in Fig. 5 were obtained for systems of sizes $N = 50, 100, 150$ at the corresponding critical mortality values $m_c(N)$. The dashed curve is the universal Bramwell, Holdsworth, and Pinton (BHP) distribution [52,53], a distribution of the Gumbel family characterizing the fluctuations of several complex systems of different nature close to criticality [52–57]. As shown by Fig. 5, $\phi_{S\mathrm{MAX}}$ exhibits at $m_c$ a strong non-Gaussian behavior with skewness independent of the system size $N$, and it is well approximated by the BHP distribution [52–55], a behavior confirming the critical character of the full desertification transition at $m_c$. From a practical point of view, the emergence of a strong non-Gaussianity, with positive skewness represents a further indicator of this transition [58].

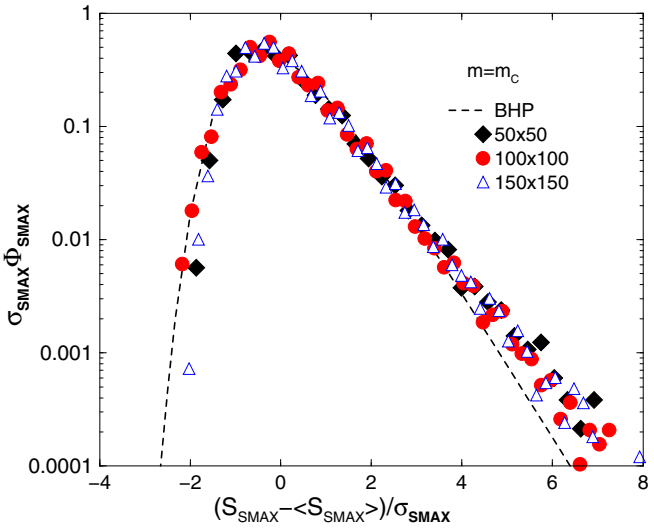


FIG. 5. (Color online) Normalized PDF of the time fluctuations of the biggest cluster size, $S_{\mathrm{MAX}}$, for $m = m_c(N)$ and different system sizes: $N = 50$ (black diamonds), $N = 100$ (red circles), and $N = 150$ (blue triangles). The dashed curve corresponds to the BHP distribution with positive skewness.

However, the full desertification transition occurs at high mortality rates, when the degradation process of the ecosystem is at a rather advanced stage. Thus, to identify early indicators we need to consider the behavior of the system for lower values of $m$.

### B. Fragmentation and desertification transitions

We consider now two other relevant ranges of mortality rate values: the first one pertains to the percolation transition of the vegetated cells, i.e., to the onset of the fragmentation of the vegetation phase. The second one is related to the percolation transition of nonliving cells, i.e., to the onset of a state in which the set of unoccupied and degraded cells percolates. We will call this transition desertification transition. Then for increasing $m$, the ecosystem goes through three kinds of transitions: *fragmentation*, *desertification*, and *full desertification* (full vegetation extinction and nearly complete soil degradation).

We stress the fact that for finite-size systems, like real-world ones, both the fragmentation and desertification transitions can be identified with intervals of mortality values instead of with a single value of $m$: the consideration of different spanning criteria characterizing the transition stages [39,40] offers a more accurate description of the ecosystem state and a tool for monitoring step by step the degradation of the system. It is then useful to consider two sets of thresholds (instead of two single thresholds): one set is associated with the percolation of living cells, the other with the percolation of nonliving ones.

Following the previous considerations, in order to analyze the vegetation fragmentation transition we computed the spanning probabilities for a cluster of living cells according to the different criteria in lattices of linear size $N = 100$. These probabilities, $R_{b+}$, $R_{h+}$, $R_{e+}$, $R_{1+}$, are plotted in Fig. 6 as functions of the average living cell density $\langle \rho_+ \rangle$. The two independent probabilities $R_{b+}$ and $R_{h+}$ were directly computed by counting the number of occurrences of an incipient spanning cluster, as described in Sec. II. The three curves $R_{b+}$, $R_{h+}$, $R_{e+}$ show similar trends, and, going from $R_{b+}$ to $R_{h+}$ and $R_{e+}$, they are progressively shifted to the left. This is consistent with the condition associated with $R_{b+}$ (simultaneous existence of a spanning cluster in both horizontal and vertical directions), more strict than the requirement of a spanning cluster in a given direction only ($R_{h+}$), or of a spanning cluster in either of the two directions

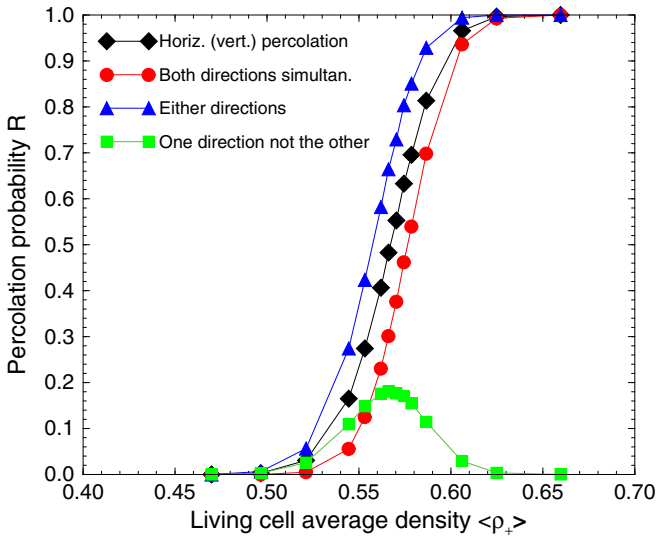


FIG. 6. (Color online) Spanning probabilities for a cluster of living cells as a function of their average density $\langle\rho_+\rangle$ corresponding to different percolation criteria: $R_h$ (black diamonds), $R_b$ (red circles), $R_e$ (blue triangles), $R_1$ (green squares) (see text).

($R_{e+}$). The percolation thresholds corresponding to these three probabilities, $p^+_{Cb}$, $p^+_{Ch}$, and $p^+_{Ce}$ were computed via Eq. (5). On the other hand, the probability $R_{1+}$ (existence of a spanning cluster in a direction but not in the other) is nonmonotonic: In this case the percolation threshold is given by the value of $\langle\rho_+\rangle$ where $R_{1+}$ attains its maximum, $p^+_{C1} = \langle\rho_+\rangle_{\max R_{1+}}$ [40]. The four thresholds and the corresponding values of $m$ are reported in Table II.

The behavior of the probabilities $R_{b0-}$, $R_{h0-}$, $R_{e0-}$, $R_{10-}$, associated with the existence of spanning clusters of nonliving cells, as function of $\langle\rho_{0,-}\rangle$ mirror their counterparts for the living cells. The percolation thresholds for nonliving cells $p^{0-}_{C1} = \langle\rho_{0,-}\rangle_{\max R_{10-}}$ and $p^{0-}_{Cb}$, $p^{0-}_{Ch}$, $p^{0-}_{Ce}$ are given in Table III.

Since both $\langle\rho_+\rangle$ and $\langle\rho_{0,-}\rangle$ depend on the mortality rate, all the probabilities $R_{b+}$, $R_{h+}$, $R_{e+}$, $R_{1+}$ (full symbols) and $R_{b0-}$, $R_{h0-}$, $R_{e0-}$, $R_{10-}$ (empty symbols) can also be plotted as functions of $m$ (Fig. 7). The steep drop in the probability values $R_{b+}$, $R_{h+}$, $R_{e+}$ and the sharp increase of $R_{b0-}$, $R_{h0-}$, $R_{e0-}$ respectively, correspond to the two intervals of values associated with the percolation thresholds of living and nonliving cells. In particular, we can define the following special values of mortality rate, corresponding to the different percolation thresholds: $m^+_b < m^+_1 < m^+_h < m^+_e$ and $m^{0-}_e < m^{0-}_h < m^{0-}_1 < m^{0-}_b$.

TABLE II. Percolation thresholds of the living cells for the different spanning criteria [39,40] and corresponding values of the mortality rate. The estimated error is ±0.0005 in both cases.

| Living cells: percolation direction | $m$ | $p^+_C$ |
|---|---|---|
| $R^b$ (both directions) | 0.1090 | 0.5879 |
| $R^1$ (only one direction) | 0.1150 | 0.5662 |
| $R^h$ (horizontal direction) | 0.1155 | 0.5646 |
| $R^e$ (either directions) | 0.1175 | 0.5554 |

TABLE III. Percolation thresholds of the nonliving cells for the different spanning criteria and corresponding values of $m$. The estimated error is ±0.0005 in both cases.

| Nonliving cells: Percolation direction | $m$ | $p^{0-}_C$ |
|---|---|---|
| $R^b$ (both directions) | 0.1450 | 0.5886 |
| $R^1$ (only one direction) | 0.1430 | 0.5785 |
| $R^h$ (horizontal direction) | 0.1410 | 0.5664 |
| $R^e$ (either directions) | 0.1405 | 0.5626 |

The curves in Fig. 7 highlight the existence of a special value of the mortality rate $m^* = 0.132 \pm 0.001$ where no phase percolates: this value corresponds to the point of maximum instability of the system and to the highest fragmentation for both phases. As the plot in Fig. 8 clearly shows, $m^*$ corresponds to the intersection point of the curves $\langle\rho_+\rangle$ and $\langle\rho_{0,-}\rangle$; i.e., it fullfils the condition: $\langle\rho_+\rangle = \langle\rho_{0,-}\rangle = 0.5$. We notice that while the particular value of $m^*$ depends on the choice of the other model parameters, $m^*$ is always characterized by the above condition associated with the maximum instability of the system. The two intervals for $m$ and the corresponding two intervals for the density values $\langle\rho_+\rangle$ and $\langle\rho_{0,-}\rangle$ defined by the percolation thresholds are also evident in Fig. 8 [respectively, vertical dashed lines and horizontal dashed lines, gray (green online) and black]. Thus, Fig. 8 illustrates a general feature of a percolative transition externally driven and occurring in finite-size systems: different spanning criteria and related different percolation thresholds define ranges of the driving parameter values in which the system progressively breaks its connectivity. The identification and empirical observation of these thresholds offer a useful tool for assessing and monitoring step by step the increasing degradation of the system.

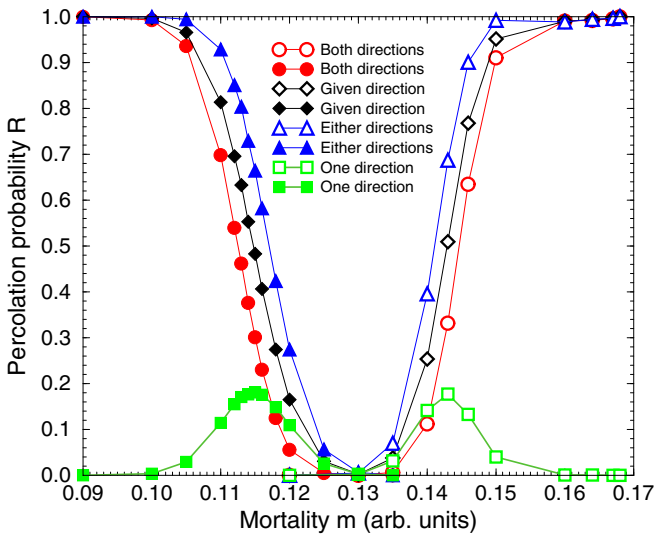


FIG. 7. (Color online) Spanning probabilities for a cluster of living cells (full symbols) and nonliving cells (empty symbols) as a function of the mortality rate $m$ for different percolation criteria: $R_h$ (black diamonds), $R_b$ (red circles), $R_e$ (blue triangles), $R_1$ (green squares).

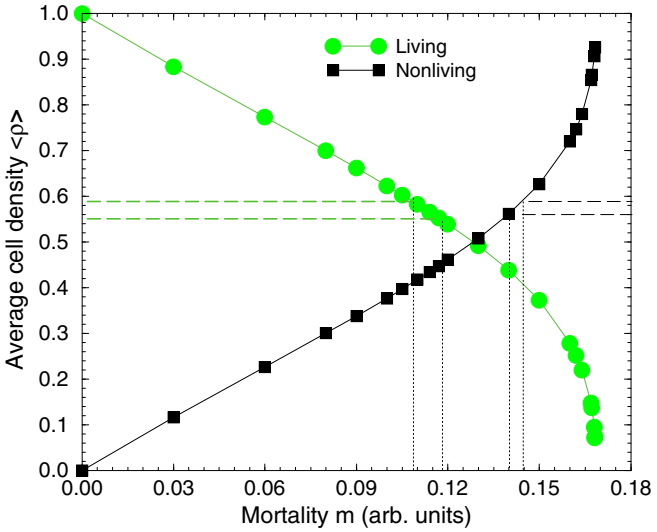


FIG. 8. (Color online) Average densities of living cells (green circles) and nonliving cells (black squares) vs $m$. The vertical and the horizontal lines identify the intervals of mortality and average density corresponding to the fragmentation and desertification transitions.

Tagging both degraded and dead cells as generically "nonliving" is useful for the percolation analysis, which can be developed in terms of two competing phases. However, as stated in Sec. II, their differentiation is one of the main features of the SCA model under consideration. In fact, the two sets of cells obey to different dynamical rules and account for different biological and geophysical roles played inside the ecosystem by regions of soil simply unoccupied or utterly degraded [1,2]. It is therefore important to keep track of the individual behavior of the two sets of cells. Figure 9 displays the average densities of the dead cells, $\langle\rho_0\rangle$, and of the degraded ones, $\langle\rho_-\rangle$, as a function of $m$, together with the plots of $\langle\rho_+\rangle$ and $\langle\rho_{0,-}\rangle$. We can see that the density of dead cells progressively increases when the system approaches the fragmentation transition (percolation of living cells) and reaches its maximum at $m \approx m_e^{0-} = 0.1405$, i.e., at the beginning of the desertification transition, when $\langle\rho_{0,-}\rangle = p_{Ce}^{0-}$ (first threshold of the nonliving phase percolation). For higher mortality rate, the fraction of dead cells decreases abruptly while that of degraded cells steps up (these cells become the dominant phase). The relatively high density of dead cells for $0.10 < m < 0.16$, in the range covering both the fragmentation and desertification transitions, is explained by the fact that dead cells are mainly located at the interface between vegetated and degraded cells. Therefore, the concentration of dead cells increases with the progressive mixing between the two phases which maximizes the roughness of the interface and thus the number of cells belonging to it. The increase in $\langle\rho_0\rangle$ provides a very early indicator of desertification.

Relevant information on the state of the system close to the fragmentation and the desertification transitions can be obtained by considering the time series of the size of the biggest cluster $S_{\mathrm{MAX}}(t)$ for living, nonliving, and degraded cells. Let $S_{\mathrm{MAX}}$ be the number of cells of a given kind in the biggest cluster divided by the total number of cells $N^2$ in the lattice. Figure 10 displays the average size $\langle S_{\mathrm{MAX}}\rangle$ as a function of the mortality rate. Precisely, the three sets of data correspond to living (light gray circles, green online), nonliving (black squares), and degraded cells (dark gray triangles, red online). From left to right, the two pairs of vertical lines point out, respectively, the two intervals of the mortality rate associated with the fragmentation and the desertification transitions.

On the left of the fragmentation interval, the circles show the average size of the biggest vegetation cluster: it spans the system both horizontally and vertically, because the average living cell density is above the highest percolation threshold $\langle\rho_+\rangle > p_{Cb}^{+}$. In the fragmentation region, limited by the first couple of dotted lines, the circles display the average size of

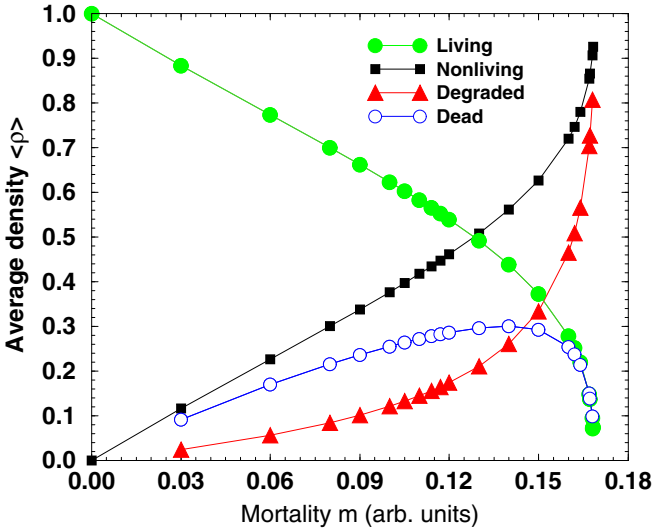


FIG. 9. (Color online) Average densities vs $m$: living cells (green circles), nonliving cells (black squares), dead cells (open blue circles), degraded cells (red triangles).

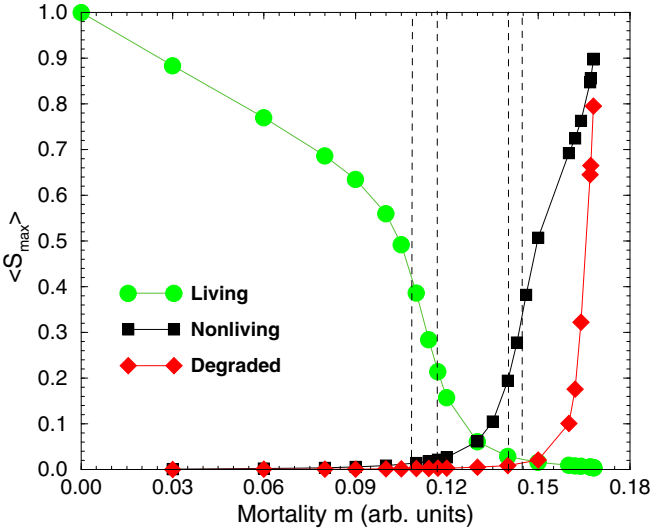


FIG. 10. (Color online) Average size of the biggest cluster $\langle S_{\mathrm{MAX}}\rangle$ vs the mortality rate: living cells (green circles), nonliving cells (black squares), and degraded cells (red triangles). The curves are a guide for the eye. The vertical lines point out the two ranges corresponding to the fragmentation and desertification transitions.

the biggest vegetation cluster spanning or not, according to the chosen spanning rule. Further right, the circles show the average size of the biggest but non spanning vegetation cluster, because the average density is below the smallest percolation threshold $\langle \rho_+ \rangle < p^+_{Ce}$. We notice that there is a steep decrease of $\langle S_{\mathrm{MAX}} \rangle$ in the fragmentation region, where a relatively small 8% variation of $m$ causes the fraction of living cells in the biggest cluster to fall from about 40% to 20%. The average size of the biggest cluster of nonliving cell mirrors this behavior: in this case, the biggest cluster size increases abruptly in the desertification region between the second pair of lines, where the average fraction of nonliving cells in the biggest cluster jumps up from about 20% to 38%, for a relatively small variation (only 4%) of $m$ (from $m = 0.140$ to $m = 0.146$). As previously explained, the percentage of dead cells in this region is significant. Finally, looking at the degraded cells, the average size of the biggest cluster abruptly increases only for higher $m$, on the right of the desertification region.

Other relevant information, including new early indicators, can be obtained from the distributions of the fluctuations $\Delta S_{\mathrm{MAX}}(t)$ for living, nonliving, and degraded cells studied as a function of the mortality rate. We start by considering their second moments. In Fig. 11 we plot the root-mean-square deviations of $\Delta S_{\mathrm{MAX}}(t)$ as a function of $m$ for the three kinds of cells. In all cases, $\sigma_{SMAX}$ has a sharp peak in the corresponding transition region, i.e., fragmentation transition for living cells (green circles), desertification transition for nonliving ones (black squares), and full desertification for degraded cells (red triangles). Precisely, the three curves reach their maxima, respectively, at $m = 0.115 \pm 0.001$, $m = 0.145 \pm 0.001$, and $m = 0.164 \pm 0.001$. Thus, $\sigma_{SMAX}$ for the biggest cluster of living cells is at a maximum for $m \approx m^+_1 \approx m^+_h \approx m^+_e$ and then decreases steeply when $\langle \rho_+ \rangle$ drops below the smallest percolation threshold $p^+_{Ce}$.

The peak of $\sigma_{SMAX}$ in the fragmentation region can be understood in the light of the results in Ref. [42], concerning

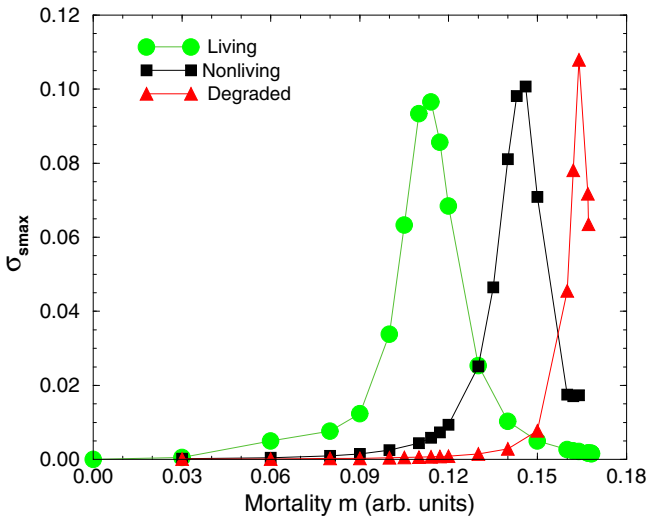


FIG. 11. (Color online) Root-mean-square deviation of $\Delta S_{\mathrm{MAX}}(t)$ vs the mortality rate. The green circles, black squares, and red triangles show the data, respectively, for living, nonliving, and degraded cells. The curves are drawn as guide for eyes.

the properties of the largest cluster for site percolation in the subcritical region ($p < p_C$). We remark that the results in Ref. [42] were obtained for an uncorrelated percolation, which is a case much simpler than the correlated process (in both space and time) that we are discussing here. However, given the complexity of our system, the uncorrelated percolation approach provides a basic frame for understanding, at least qualitatively, the overall properties of the biggest clusters in the correlated case. In particular, we refer to the following estimate in Ref. [42] of the standard deviation of the fluctuations $\Delta S_{\mathrm{MAX}}(t)$ in the subcritical density region, for $N \to \infty$:

$$\frac{\sigma_{SMAX}}{s^*_\xi} \sim \frac{\pi}{\sqrt{6}} + \epsilon_N. \tag{8}$$

In Eq. (4) $s^*_\xi$ is the effective crossover size [42]; $s^*_\xi \sim s_\xi$, where $s_\xi$ is the usual crossover size [37,38] controlling the exponential decay of the cluster size distribution for $p < p_C$:

$$n_s \sim s^{-\theta} e^{-s/s_\xi}, \tag{9}$$

while $\epsilon_N$ is a periodic function of $\log N$ with period $1/s^*_\xi$ [42]. Then the discussion of the uncorrelated percolation case points out the relation between the root-mean-square deviation of the fluctuations of the biggest cluster size, $\sigma_{SMAX}$, considered here, and two other quantities, widely studied in percolation theory, such as the crossover size $s_\xi$ and the average cluster size $\chi$ [37,38]. They both diverge at $p_c$ for $N \to \infty$: $s_\xi \propto |p - p_C|^{-1/\sigma}$ and $\chi \propto |p - p_C|^{-\gamma}$; for finite-size systems, they present a peak of finite height and width [37,38].

In our finite-size system, the peak of $\sigma_{SMAX}$ observed close to the percolation thresholds suggests that it can be used as a very early indicator of transition in applications to real world cases. In fact, looking at the fragmentation and the desertification transition regions in Fig. 11 (corresponding to percolation of living and nonliving cells, respectively) we observe that the maxima of $\sigma_{SMAX}$ are attained at the thresholds values of $m$, but a significant increase of $\sigma_{SMAX}$ occurs earlier, *well before the system crosses these thresholds*, i.e., at $\langle \rho_+ \rangle > p^+_{Cb}$ for the fragmentation transition and $\langle \rho_{0,-} \rangle < p^{0,-}_{Ce}$ for the desertification transition. Moreover, even if for a finite-size system the height and width of the peak depend on $N$ (and thus the precise values of $\sigma_{SMAX}$ close to the percolation thresholds depend on $N$), $\sigma_{SMAX}$ will always increase before the transition threshold for every finite $N$. Consequently the growth of $\sigma_{SMAX}$ represents a very early indicator of transition, definitely earlier of the emergence of the exponential cutoff in the cluster size distribution, Eq. (5), as proposed in Ref. [9]. In particular, the increase of $\sigma_{SMAX}$ for the size fluctuations of the biggest living cluster provides an early and sensitive indicator for the fragmentation transition [58], while the growth of $\sigma_{SMAX}$ for the biggest nonliving cluster is an early (and sensitive) indicator of desertification. Both these indicators can be used in real-world applications, which are usually characterized by relatively short empirical time series. In fact, the relative error on $\sigma_{SMAX}$ calculated for a time series of length $L$ is $\frac{1}{2\sqrt{L}}\sqrt{2+k}$, where $k$ is the (finite) kurtosis of the distribution $\phi_{SMAX}$ [59]. A simulation of the effect of the time series length on $\sigma_{SMAX}$ is shown in Fig. 12.

The importance of the biggest cluster as a promising source for indicators of transition is confirmed when considering

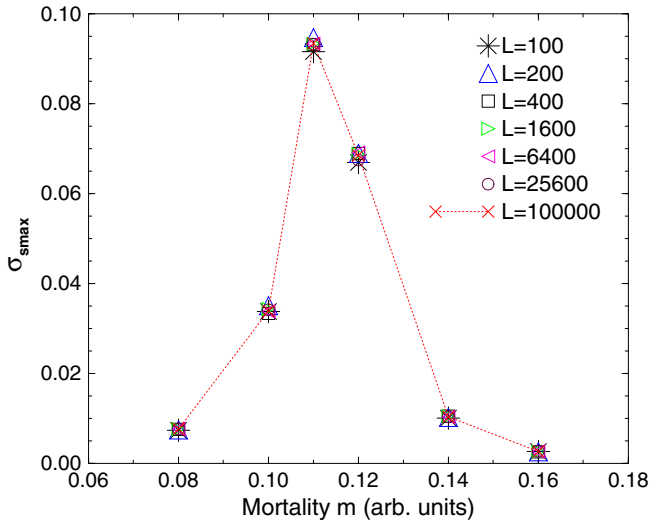


FIG. 12. (Color online) Root-mean-square deviation $\sigma_{SMAX}$ for living cells vs the mortality rate, calculated for times series of different length $L$. The values $\sigma_{SMAX}(t)$ are obtained by averaging over $N_L$ realizations of the time series (for $L = 100$ $N_L = 256$, for $L = 200$ $N_L = 128$, for $L = 400$ $N_L = 64$, for $L = 800$ $N_L = 32$, for $L = 1600$ $N_L = 16$, for $L = 6400$ $N_L = 4$, for $L = 12800$ $N_L = 2$, for $L = 25\,600$ and $L = 100\,000$ $N_L = 1$). The curve is drawn as guide for the eye.

two other properties of its size fluctuations given by the statistics of the return times of extreme values and the PDF of the fluctuation distribution. Figure 13 shows a window in the time series $S_{MAX}(t)$ of the biggest cluster of living cells for $m = 0.08$, a mortality level well below the lowest threshold $m_b^+$. The figure displays a strong non-Gaussianity marked by a pronounced asymmetry between downward and upward fluctuations, which can be measured by the return times of extreme values. More precisely, we considered the return times of extreme values of the normalized time series

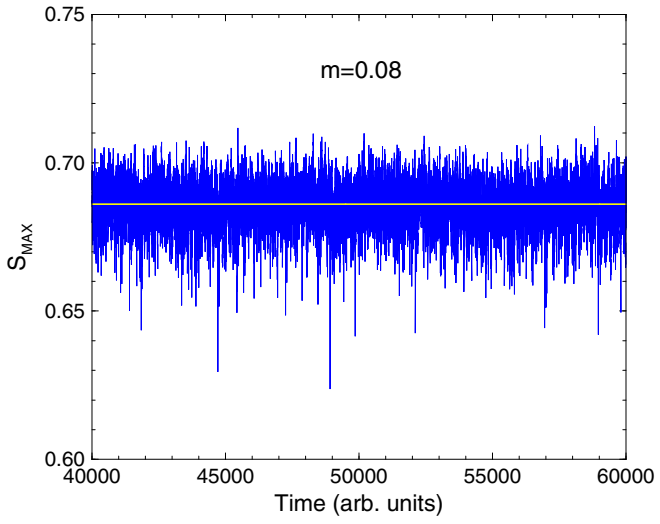


FIG. 13. (Color online) Size of the biggest cluster of living cells vs time for $m = 0.08$. The time unit is one iteration step. The white (yellow) line is the average value. Only a small time window of the full $S_{MAX}$ time series is displayed.

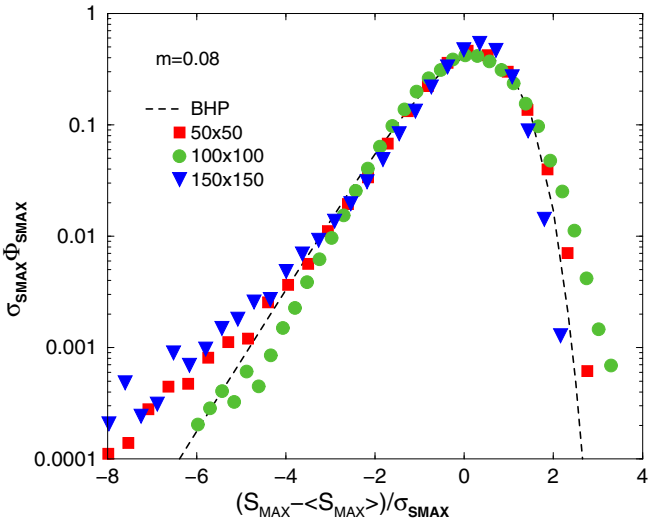


FIG. 14. (Color online) Normalized PDF of the time fluctuations of the biggest cluster size $S_{MAX}$ for living cells, $m = 0.08$ and different system sizes: $N = 50$ (red squares), $N = 100$ (green circles), and $N = 150$ (blue triangles). The dashed curve corresponds to the BHP distribution with negative skewness.

with zero average and unitary variance given by $S'_{MAX}(t) \equiv \Delta S_{MAX}(t)/\sigma_{SMAX}$. Following Refs. [60–63], we computed the return times of high threshold values $q_{S'}$ (in units of $\sigma_{SMAX}$), i.e., the time intervals between two consecutive occurrences of the events $S'_{MAX}(t) > q_{S'}$. We found that for a time series with $10^5$ records this condition is fulfilled $N_q = 573$ times for the negative threshold $q_{S'} = -3.0$ (average return time $R_q = 174.5$) but only $N_q = 37$ times for the positive threshold $q_{S'} = 3.0$ (average return time $R_q = 2702.7$).

This strong asymmetry between the average return times of negative and positive extreme values of $S'_{MAX}$ at $m = 0.08$ accounts for a significant negative skewness of the fluctuation distribution of $S_{MAX}(t)$, evident in Fig. 14 where a normalized representation of the PDF at $m = 0.08$ is plotted for different system sizes. The dashed curve represents the universal BHP distribution with negative skewness [52–55] reported here for comparison. We notice that the PDF in Fig. 14 is consistent with the result in Ref. [42] for the cumulative distribution function of the largest cluster size obtained for uncorrelated percolation. Moreover, considering $\phi_{SMAX}$ for the biggest living cluster as a function of $m$, we found that for small mortality rates (up to $m \approx 0.06$) the distribution is Gaussian (hence with zero skewness). At higher $m$, the PDF acquires a negative skewness, progressively increasing in absolute value. This trend persists until $m \approx 0.10$ where the skewness reaches its minimum value. A further increase of $m$ brings the systems close the threshold $m_b^+$ associated with the disappearance of a living cluster spanning in both (horizontal and vertical) directions simultaneously. For $m > 0.10$ the skewness starts to increase, and it becomes near zero in the fragmentation region $m_b^+ < m < m_b^e$. For $m > m_b^e$, no spanning cluster of living cells exists and $\phi_{SMAX}$ develops a positive and progressively increasing skewness which reaches its maximum at $m_c$, the extinction threshold (Fig. 5).

Therefore, concerning the identification of new early transition indicators, the skewness of the distribution of

$\Delta S_{\mathrm{MAX}}(t)$ for the biggest cluster of vegetation has good potential since its analysis suggests two indicators of the fragmentation transition: (1) the emergence of a negative skewness of the distribution at relatively low mortality rate below the fragmentation threshold (a very early indicator of the fragmentation transition); and (2) the change of sign in the skewness, from negative to positive, occurring at the fragmentation threshold.

On the other hand, the opposite behavior characterizes the distribution of the fluctuations of the nonliving biggest cluster at increasing $m$: the skewness is zero for small $m$ (where the distribution is Gaussian) and then becomes positive and finally negative. Thus, we can propose two new indicators also for the desertification transition: (1) the very early appearance of a positive skewness and (2) the change of sign in the skewness, from positive to negative.

## IV. CONCLUSIONS

We have presented in this paper a theoretical study of the desertification transitions in semiarid or arid ecosystems. We simulated the degradation of the ecosystem by making use of a stochastic cellular automaton model [10], and we analyzed the results for the dynamics of the vegetation clusters in terms of percolation theory, assumed as an effective tool for analyzing the geometrical properties of the clusters [37–39].

By considering the full range of values of the mortality rate, the parameter setting the strength of external stresses, assumed as driving parameter of the transition, we can follow the increasing degradation of the ecosystem going from the vegetation fragmentation transition, occurring at moderate values of $m$ and characterized by the disappearance of a vegetation cluster spanning the whole system, up to the desertification transition, associated with the emergence of a spanning cluster of empty and degraded soil regions, and finally, to the full desertification transition, corresponding to the full extinction of the vegetation cover and the nearly complete degradation of the soil. We found that the application of the percolation framework for the analysis of the desertification risk of an ecosystem offers a powerful tool for the identification of several new and early transition indicators.

The desertification process considered in this paper is associated with a critical transition, as we pointed out by analyzing the full desertification transition. For this last we found a continuous power-law decrease of the average living cell density $\langle \rho_+ \rangle$ which approaches the extinction threshold and a power-law increase of the root-mean-square deviation of the $\rho_+$ fluctuations, $\sigma_{\rho_+}$. Both power laws are associated with nonuniversal critical exponents $\beta$ and $\gamma'_\sigma$ [46]. Since the model leads to different kinds of transitions in different regions of the parameter space [9], the continuous character of the transition discussed here depends on the choice of the parameters. The values adopted in this work were taken as a reasonable starting point to simulate "real-world" field data [9,19]. The application of the percolation analysis to the case of abrupt (first-order) transitions is left to further investigations. From a practical point of view, we notice that both the steep increase of $\sigma_{\rho_+}$ and the pronounced positive skewness of $\phi_{S\mathrm{MAX}}$ at high $m$ provide indicators for the full desertification transition.

For what concerns the fragmentation and desertification transitions, the existence of several percolation thresholds associated with different spanning criteria [39–41] and corresponding to well-defined numerical intervals for the driving parameter provides a way to closely follow the progressive degradation of the system, marked, step by step, by the different thresholds.

An important result of our analysis is that it highlights the effectiveness of studying the size fluctuations of the biggest clusters of both living and nonliving cells. This study points out the role played by the increase of $\sigma_{S\mathrm{MAX}}$ as early transition indicator: the maxima are in fact attained in the transition regions (fragmentation transition for the biggest vegetation cluster and desertification transition for the biggest nonliving cluster). Finally, other new and early indicators of transition are obtained by the analysis of the PDF of the fluctuations $\Delta S_{\mathrm{MAX}}(t)$ for both the biggest clusters. In particular, the change of sign in the skewness (from negative to positive) for the distribution of $\Delta S_{\mathrm{MAX}}(t)$ of the biggest vegetation cluster is associated with the fragmentation threshold, while the reverse change of sign (from positive to negative) occurs at the desertification threshold for the distribution of the size fluctuations of the biggest nonvegetated cluster.

Overall our results offer new insights on the desertification transitions occurring at increasing mortality rates in semiarid or arid ecosystems, going through stages characterized by an increasing loss of connectivity in the vegetation and degradation of the soil. The identification of new transition indicators related to these stages, including very early ones, can greatly help to monitor the degradation processes in fragile ecosystems.

## ACKNOWLEDGMENTS

A.M.C. thanks the members of the Dynamical System Group (DynamIC) at the Department of Mathematics of Imperial College London, for friendly and fruitful collaboration during her academic visit. R.C. thanks the support of the Euro-Mediterranean Centre for Climate Change (CMCC), Italy. All the authors thank Prof. Silvano Marchiori and Prof. Piero Lionello of the Department of Biotechnology and Environmental Science, University of Salento, for helpful comments and valuable discussions.

[1] *Ecosystems and Human Well-Being: Synthesis, Millennium Ecosystem Assessment Series*, edited by J. Sarukhán and A. Whyte (Island Press, Washington, DC, 2005).

[2] R. M. M. Crawford, *Plants at the Margin, Ecological Limits and Climate Change* (Cambridge University Press, Cambridge, 2008).

[3] W. H. Schlesinger, J. F. Reynolds, G. L. Cunningham, L. F. Huenneke, W. M. Jarrell, R. A. Virginia, and W. G. Whitford, Science **247**, 1043 (1990).

[4] J. F. Reynolds, D. M. Stafford Smith, E. F. Lambin, B. L. Turner II, M. Mortimore, S. P. J. Batterbury, T. E. Downing, H. Dowlatabadi, R. J. Fernández, J. E. Herrick, E. Huber-Sannwald,

H. Jiang, R. Leemans, T. Lynam, F. T. Maestre, M. Ayarza, and B. Walker, Science **316**, 847 (2007).
[5] E. Pennisi, Science **341**, 482 (2013).
[6] N. S. Diffenbaugh and C. B. Field, Science **341**, 486 (2013).
[7] J. L. Blois, P. L. Zarnetske, M. C. Fitzpatrick, and S. Finnegan, Science **341**, 499 (2013).
[8] R. V. Solé and J. Bascompte, *Self-organization in Complex Ecosystems* (Princeton University Press, Princeton, 2006).
[9] S. Kéfi, M. Rietkerk, C. L. Alados, Y. Pueyo, V. P. Papanastasis, A. ElAich, and P. C. de Ruiter, Nature (London) **449**, 213 (2007).
[10] S. Kéfi, M. Rietkerk, M. van Baalen, and M. Loreau, Theor. Popul. Biol. **71**, 267 (2007).
[11] J. von Hardenberg, E. Meron, M. Shachak, and Y. Zarmi, Phys. Rev. Lett. **87**, 198101 (2001).
[12] N. M. Shnerb, P. Sarah, H. Lavee, and S. Solomon, Phys. Rev. Lett. **90**, 038101 (2003).
[13] M. Scheffer, S. R. Carpenter, T. M. Lenton, J. Bascompte, W. Brock, V. Dakos, J. van de Koppel, I. A. van de Leemput, S. A. Levin, E. H. van Nes, M. Pascual, and J. Vandermeer, Science **338**, 344 (2012).
[14] V. Dakos, S. R. Carpenter, W. Brock, A. M. Ellison, V. Guttal, A. R. Ives, S. Kéfi, V. Livina, D. A. Seekell, E. H. van Nes, and M. Scheffer, PLoS ONE **7**, e41010 (2012).
[15] S. Kéfi, V. Dakos, M. Scheffer, E. H. van Nes, and M. Rietkerk, Oikos **122**, 641 (2013).
[16] V. Dakos, S. Kéfi, M. Rietkerk, E. H. van Nes, and M. Scheffer, Am. Nat. **177**, e153 (2011).
[17] R. Donangelo, H. Fort, V. Dakos, M. Scheffer, and E. H. van Nes, Int. J. Bifurcat. Chaos **20**, 315 (2010).
[18] V. Dakos, E. H. van Nes, R. Donangelo, H. Fort, and M. Scheffer, Theor. Ecol. **3**, 163 (2010).
[19] S. Kéfi, V. Guttal, W. A. Brock, S. R. Carpenter, A. M. Ellison, V. N. Livina, D. A. Seekell, M. Scheffer, E. H. van Nes, and V. Dakos, PLoS ONE **9**, e41010 (2014).
[20] G. P. Asner, D. E. Knapp, A. Balaji, and G. Páez-Acosta, J. Appl. Remote Sens. **3**, 033543 (2009).
[21] S. Palminteri, G. W. N. Powell, G. P. Asner, and C. A. Peres, Remote Sens. Environ. **127**, 98 (2012).
[22] S. R. Levick and G. P. Asner, Biol. Conserv. **157**, 121 (2013).
[23] K. M. Dahlin, G. P. Asner, and C. B. Field, Proc. Natl. Acad. Sci. USA **110**, 6895 (2013).
[24] G. P. Asner, J. R. Kellner, Ty Kennedy-Bowdoin, D. E. Knapp, C. Anderson, and R. E. Martin, PLoS ONE **8**, e60875 (2013).
[25] M. Zampieri and P. Lionello, Climate Res. **41**, 205 (2010).
[26] M. Scheffer, J. Bascompte, W. A. Brock, V. Brovkin, S. R. Carpenter, V. Dakos, H. Held, E. H. van Nes, M. Rietkerk, and G. Sugihara, Nature (London) **461**, 53 (2009).
[27] V. Dakos, M. Scheffer, E. H. van Nes, V. Brovkin, V. Petoukhov, and H. Held, Proc. Natl. Acad. Sci. USA **105**, 14308 (2008).
[28] V. Guttal and C. Jayaprakash, Theor. Ecol. **2**, 3 (2009).
[29] T. M. Scanlon, K. K. Caylor, S. A. Levin, and I. Rodriguez-Iturbe, Nature (London) **449**, 209 (2007).
[30] M. Rietkerk, S. C. Dekeer, P. C. de Ruiter, and J. van de Koppel, Science **305**, 1926 (2004).
[31] S. R. Carpenter and W. A. Brock, Ecol. Lett. **9**, 311 (2006).
[32] V. Guttal and C. Jayaprakash, Ecol. Lett. **11**, 450 (2008).
[33] L. Telesca, R. Lasaponara, and A. Lanorte, Physica A **361**, 699 (2006).
[34] A. Manor and N. M. Shnerb, Phys. Rev. Lett. **101**, 268104 (2008).
[35] A. Manor and N. M. Shnerb, Phys. Rev. Lett. **103**, 030601 (2009).
[36] A. Ilachinski, *Cellular Automata: A Discrete Universe* (World Scientific, Singapore, 2002).
[37] D. Stauffer and A. Aharony, *Introduction to Percolation Theory* (Taylor & Francis, London, 1992).
[38] K. Christensen and N. R. Moloney, *Complexity and Criticality* (Imperial College Press, London, 2005).
[39] J. P. Hovi and A. Aharony, Phys. Rev. E **53**, 235 (1996).
[40] M. E. J. Newman and R. M. Ziff, Phys. Rev. Lett. **85**, 4104 (2000).
[41] R. M. Ziff and M. E. J. Newman, Phys. Rev. E **66**, 016129 (2002).
[42] M. Z. Bazant, Phys. Rev. E **62**, 1660 (2000).
[43] S. Kéfi, *Reading the Signs: Spatial Vegetation Patterns, Arid Ecosystems and Desertification* (Gildeprint Drukkerijen, Enschede, the Netherlands, 2008).
[44] J. Hoshen and R. Kopelman, Phys. Rev. B **14**, 3438 (1976).
[45] R. Corrado, A. M. Cherubini, and C. Pennetta (unpublished).
[46] R. Corrado, A. M. Cherubini, and C. Pennetta, Comm. Nonlinear Sci. Numer. Simul. (to be published).
[47] G. Ódor, Rev. Mod. Phys. **76**, 663 (2004).
[48] M. Henkel, H. Hinrichsen, and S. Lũbeck, *Non-Equilibrium Phase Transitions* (Springer, Berlin, 2008).
[49] H. Hinrichsen, Adv. Phys. **49**, 815 (2000).
[50] M. A. Munoz, R. Dickman, A. Vespignani, and S. Zapperi, Phys. Rev. E **59**, 6175 (1999).
[51] S. Lũbeck, J. Stat. Phys. **123**, 193 (2006).
[52] S. T. Bramwell, P. C. W. Holdsworth, and J. F. Pinton, Nature (London) **396**, 552 (1998).
[53] S. T. Bramwell, K. Christensen, J. Y. Fortin, P. C. W. Holdsworth, H. J. Jensen, S. Lise, J. M. López, M. Nicodemi, J. F. Pinton, and M. Sellitto, Phys. Rev. Lett. **84**, 3744 (2000).
[54] M. Clusel, J. Y. Fortin, and P. C. W. Holdsworth, Phys. Rev. E **70**, 046112 (2004).
[55] S. T. Bramwell, Nature Phys. **5**, 444 (2009).
[56] C. Pennetta, E. Alfinito, L. Reggiani, and S. Ruffo, Physica A **340**, 380 (2004).
[57] C. Pennetta, E. Alfinito, L. Reggiani, and S. Ruffo, Semicond. Sci. Technol. **19**, S164 (2004).
[58] R. Corrado, A. M. Cherubini, and C. Pennetta, in *Noise and Fluctuations (ICNF) 22nd International Conference*, edited by J. M. Routoure, L. Varani, and F. Pascal (IEEE, New York, 2013).
[59] J. P. Bouchaud and M. Potters, *Theory of Financial Risk and Derivative Pricing, from Statistical Physics to Risk Management* (Cambridge University Press, Cambridge, 2003).
[60] E. G. Altmann and H. Kantz, Phys. Rev. E **71**, 056106 (2005).
[61] A. Bunde, J. F. Eichner, J. W. Kantelhardt, and S. Havlin, Phys. Rev. Lett. **94**, 048701 (2005).
[62] C. Pennetta, Eur. Phys. J. B **50**, 95 (2006).
[63] L. Palatella and C. Pennetta, Phys. Rev. E **83**, 041102 (2011).